Nanoparticle Assembly by Nanoxerography

Chad R. Barry, Nyein Z. Lwin, Michael G. Steward, Heiko O. Jacobs*

Department of Electrical and Computer Engineering, University of Minnesota,
200 Union Street SE, Minneapolis, Minnesota 55455
**corresponding author, hjacobs@ece.umn.edu.*

ABSTRACT: This article reports on the electrostatic driven self-assembly of nanoparticles onto charged surface areas (receptors) with a resolution of 200 nm from the liquid-phase and 100 nm from the gas-phase. The charged areas required for this type of nanoxerographic printing were fabricated using a parallel method that employs a flexible, electrically conductive, electrode to charge a thin-film electret. As electrodes, we used metal-coated polymeric stamps and 10 micrometer thick doped silicon wafers carrying a pattern in topography. Areas as large as 1 square centimeter were patterned with charge with 100 nanometer resolution in 10 seconds. Nanoparticles assembled onto these charged receptors in 10 seconds by a liquid-phase assembly process where electrostatic forces compete with disordering forces due to ultrasonication. A first nanoxerographic printer to print nanoparticle form the gas-phase was developed as well. The printer uses a transparent particle assembly module designed to direct and monitor the assembly of nanoparticles. The electrostatically directed assembly of 10 – 100 nm sized metal (gold, silver, indium), and 30 nm sized carbon particles was accomplished with a resolution 500-1000 times greater than the resolution of existing xerographic printers.

1. INTRODUCTION

Nanoparticles can provide a variety of functions and are considered as building blocks of future nanotechnological devices. Nanoparticles are typically created in the gas or liquid-phase. Most well known techniques include metal evaporation, laser ablation, solution vaporization, wire explosion, pyrolysis, colloidal and electrochemical synthesis, and generation from plasmas. Silicon nanoparticles generated by silane pyrolysis or electrochemical reaction of hydrogen-fluoride with hydrogen-peroxide are used for non-volatile memories[1], lasers[2], and biological markers[3]. Evaporated gold[4], indium[5], and ion sputtered aluminum[6] nanoparticles are used for single electron transistors; and electron beam evaporated gold and silver particles are used for plasmonic waveguides[7]. The use of nanoparticles as building blocks, regardless of the application, requires new assembling strategies. Most actively studied approaches include: i) single particle manipulation[8], ii) random particle deposition[5], and iii) parallel particle assembly- based on self-assembly[9-16].

Stimulated by the success of atomic force based charge patterning, Wright and Chetwynd suggested in 1998 that high resolution charge patterns could be used as templates for self-assembly and as nucleation sites for molecules and small particles [14]. Since then, several serial charge-patterning processes have been explored to enable the positioning of nanoparticles. Serial techniques, however, remain slow -- the fastest scanning probe-based system needs 1.5 days to pattern an area of 1 cm^2.[17] As a new direction, we have developed a parallel charge patterning process[16] enabling nanoxerographic printing[18]. The printing technique, referred to as electric nanocontact printing, generates a charge pattern based on the same physical principles used in scanning probes but forms multiple electric nanocontacts of different size and shape to transfer charge in a single step. With this method, we demonstrated patterning of charge with 100 nm scale resolution and transfer of 50 nm to 20 μm sized particles including iron oxide, graphitized carbon, iron beads, and Xerox toner from a powder, gas, and liquid phase[16,18].

In this article we demonstrate charge pattering using flexible thin silicon electrodes and improved nanoxerographic printing strategies from the liquid and the gas phase. Previous results have been published elsewhere [18,19]. In particular we demonstrate Nanoxerographic printing with a resolution of 200 nm from the liquid-phase and 100 nm from the gas-phase, which is 500-1000 times the resolution of traditional xerographic printers [20,21].

2. EXPERIMENTAL

The electric nanocontact printing process to generate charge patterns is illustrated in Figure 1. In our experiments we tested two different flexible electrodes to accomplish charge transfer. The first electrode prototype was made out of a 5 mm thick poly-(dimethylsiloxane) (PDMS) stamp that was fabricated from a silicon mold defined by e-beam lithography.[22] The second electrode prototype was made from a 2 inch in diameter, 10 μm thick, n-doped silicon wafer (Virginia Semiconductors) patterned by phase-shift lithography, [23] etched in a 98% CF_6, 2% O_2 plasma and supported on a Au coated flat slab of PDMS. The PDMS electrode was coated with a 60 nm thick layer of gold by thermal evaporation to provide electrical conductivity. The thin silicon electrode is sufficiently conductive and does not require a metal coating.

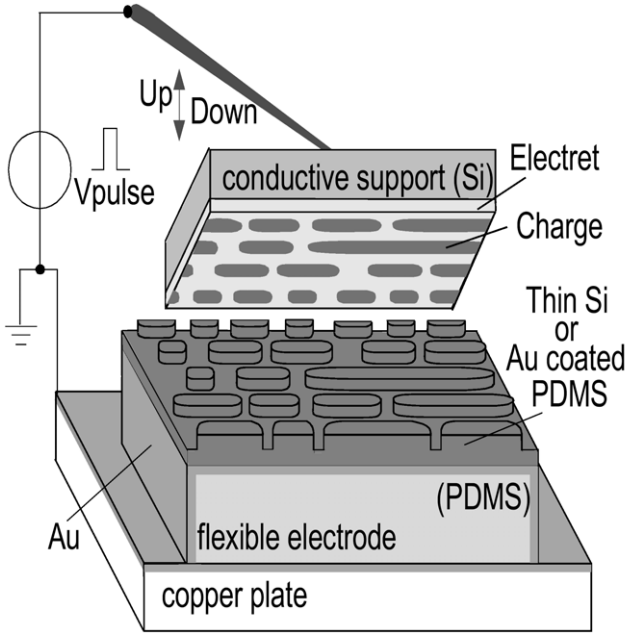

Figure 1: Principle of parallel charge patterning: A silicon chip carrying a thin film electret is placed on top of a flexible electrode supported by PDMS on a copper plate. A needle, attached to a micromanipulator is used to form an electric contact to the backside of the silicon chip. An external voltage is used to transfer a pattern of charge into the electret material at the areas of contact. The silicon chip is removed with the electret carrying a charge pattern.

As the charge storage medium, we used a 60 nm thick film of PMMA on <100> silicon wafers. The film was formed by spin coating a 2% solution of 950 K (PMMA) in chlorobenzene (MicroChem Co.) at 5000 rpm and baking it in an oven at 90 °C for 1 hour. The chips were placed on the flexible electrode by hand and contacted from the back with a metallic needle attached to a micromanipulator. To generate a pattern of trapped charge, we applied an external potential for 10 seconds. During the exposure, we monitored the current flow and adjusted the voltage (5 – 20 V) to get an exposure current of 0.1 – 1 mA. After exposure, we removed and characterized the charge patterns using Kelvin Probe Force Microscopy (KFM).[24,25]

The nanoxerographic process to direct the assembly of nanoparticles is illustrated in figure 2. The liquid-phase assembly process depicted on the left uses sonication to disperse commercially available nanoparticles in a non-polar solvent such as Perfluorodecalin and Fluorinert FC-77. Both solvents have a relative dielectric constant of 1.8 and work equally well. In the liquid-phase, we tested silica beads, < 200 nm in size, red iron-oxide particles, < 500 nm in size, and graphitized carbon nanoparticles, 30 nm in size. The silica beads were obtained from Bangs Laboratories in an aqueous solution and subsequently dried. The iron-oxide and graphite particles were obtained from PolyScience (Niles, Illinois) in the form of a powder. The powder contained loosely bound aggregates of primary particles. To assemble the nanoparticles, we place the chip carrying a charge pattern into a vial that contains 1 mL of solvent that is being sonicated using an ultrasonic bath. Subsequently, we placed a large particle aggregate, <500 μm in size for red iron oxide and graphized carbon, into the solvent. The sonication breaks up the aggregate and small particles disperse and align on the charged surface areas within seconds. The dispersion becomes visible due to a slight color change in the assembly solution. Immediately (~2 seconds) after the dispersion is recognized, the chip is removed and dried under nitrogen. The entire assembly process takes only 5 - 10 seconds. This process provided higher resolution and selectivity than assembly without sonication.

The gas-phase assembly process (Fig. 2C, D) depicted on the right uses a particle assembly module to accomplish the directed assembly of nanoparticles from the gas phase. The assembly module (Fig. 2C) consists of a cavity that holds the sample, two electrodes to generate a global electric field that directs incoming charged particles towards the sample surface, and an electrometer to count the charge of the assembled particles. This module is attached to a tube furnace (Fig. 2D) that generates the nanoparticles by evaporation and condensation.

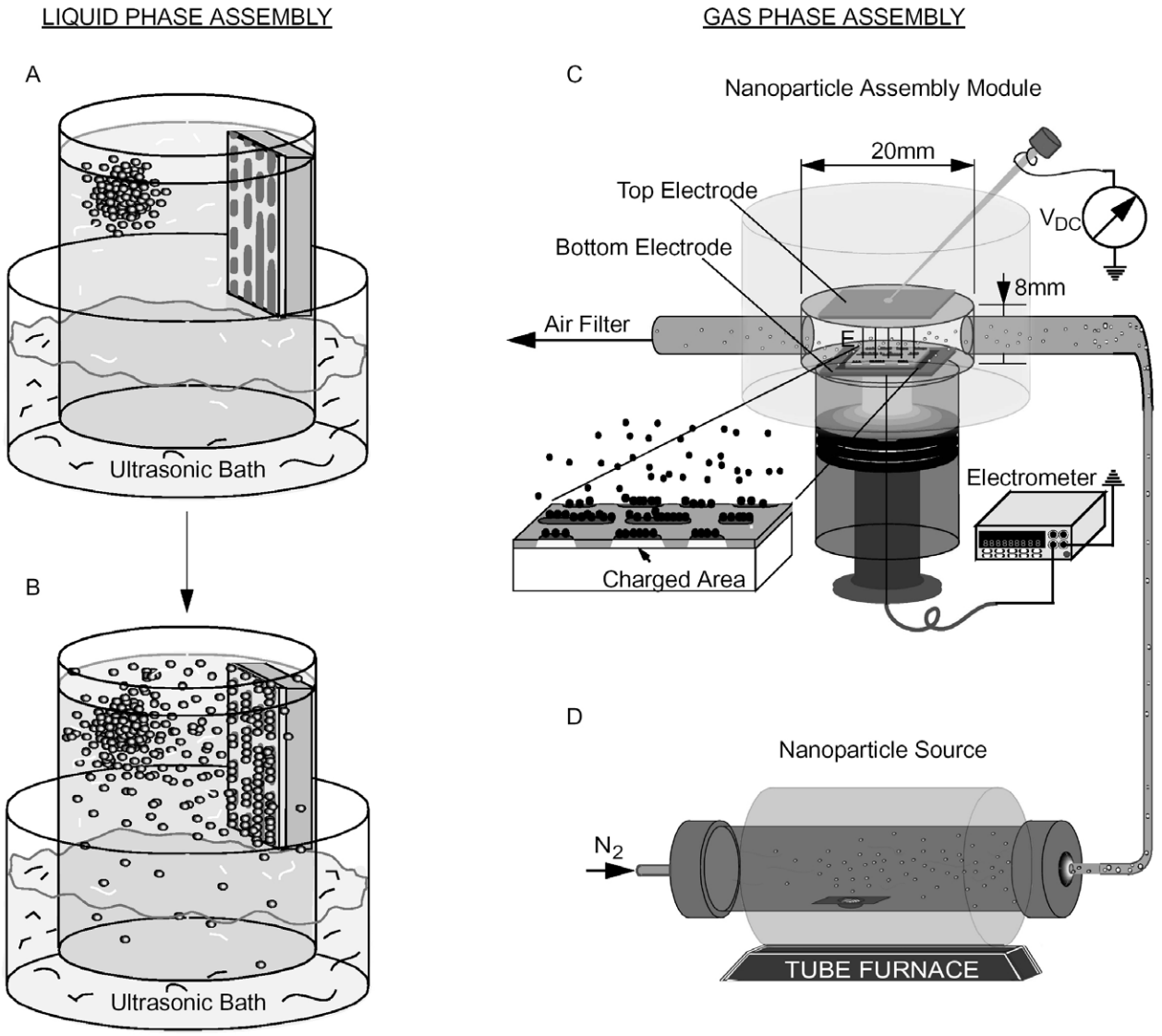

Figure 2: Principle of nanoxerographic printing from the liquid and gas phase. Liquid Phase: (A) The chip carrying a charge pattern is immersed in the solvent under sonication. A ~500 μm large aggregate of graphitized carbon nanoparticles is placed in the solvent. (B) The graphitized carbon nanoparticles disperse in the solvent and assemble on the charged areas of the chip. Gas Phase: (C) The directed assembly of the nanoparticles occurs in the particle assembly module. An external potential, V_{DC}, applied to the top electode directs incoming nanoparticles to the charged sample surface. The electrometer measures the amount of assembled, charged particles during the assembly process. (D) A constant flow of nanoparticles is generated by evaporation of matter in the tube furnace, transport of the atoms to the outlet by the N2 gas, and condensation.

The particle assembly module was constructed mainly out of PDMS. PDMS is transparent and can be molded around readily available objects in successive steps to form 3-dimensional structures. In the first step, we formed the cavity by molding PDMS around a 20 mm in diameter and 8 mm tall disk that was removed after curing the PDMS at 60 °C. In the second step, we formed a sample exchange unit by attaching a rigid polyethylene tube to the cavity using PDMS. The tube holds a retractable cylinder that carries the sample. To form a particle inlet and outlet we inserted a stainless steel tube 5mm in diameter into each side of the PDMS shell.

To direct the assembly of incoming charged particles we integrated two electrodes into the transparent assembly module. A 2 cm long and 1 cm wide electrode located at the top of the cavity and a 1.5 cm by 1 cm wide electrode underneath the sample. During operation, the electrodes are spaced by ~7 mm and we apply an external voltage of up to $\pm$1000V to bring charged particles of one polarity into the proximity of the charged sample surface.

To monitor the amount of particles that assembled onto the sample under different assembly conditions we implemented a faraday cup in the assembly module. In our faraday cup arrangement, the sample forms the cup electrode and is connected to ground with the electrometer (Keithley 6517A) in between. During assembly, image charges flow from the ground through the electrometer into the sample to the location of assembled, charged particles. As a result, the electrometer measures the accumulated charge of the assembled particles.

The particles were generated in a tube furnace. The material to be evaporated is placed inside the quartz tube at the center of the furnace. Pure nitrogen is the carrier gas that flows through the system during operation. The evaporation was carried out at 1100 °C for gold and silver, and 1000 °C for indium. A vapor containing atoms of the evaporated material forms within the furnace. The nitrogen carrier gas transports the atoms out of the furnace where they nucleate and condense into particles due to the change in temperature. The gas flow carries the nanoparticles into the particle assembly module through a 1-meter long Tygon tube.

3. RESULTS AND DISCUSSION

Representative patterns of localized charge in PMMA recorded by KFM are illustrated in Figure 3 (left) along with atomic force microscope images of the topography of the electrode structures (right) used to generate the charge patterns. Fig. (3A) shows the surface potential for a surface that was patterned with 300 nm (FWHM) wide parallel lines using a thin silicon electrode. Fig. (3B) shows 150 nm wide ring patterns generated with a PDMS electrode structure that had a recessed center of 20 nm. This demonstrates that high aspect ratio electrode structures are not required for pattern transfer. Pattern transfer occurs only at the contact areas. Both charge patterns were written by exposing the PMMA film locally with a current

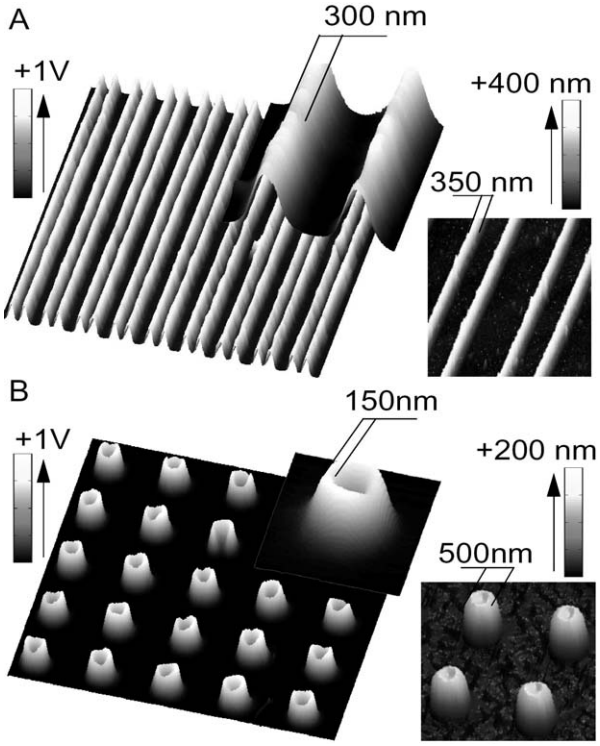

Figure 3: Kelvin probe force microscopy images of patterns of positive charge (left) in PMMA and corresponding atomic force microscope images of the topography of the electrode structures (right) used to generate the charge patterns. (A) Surface potential image of 300 nm (FWHM) positively charged parallel lines generated using a thin silicon electrode (B) Surface potential image of 150 nm wide positively charged rings generated using a PDMS electrode.

density of 1 mA/cm^2 for 10 seconds with the electrode positive. The recorded surface potential is proportional to the density of trapped charges. For the recorded potential difference we estimated that a 100 nm by 100 nm sized receptor contains 100 elementary charges.

These charge patterns attract nanoparticles. Figure 4 shows representative images of nanoxerographic printing of nanoparticles from the liquid-phase. The images show patterns of graphitized carbon trapped at charged areas on PMMA. The patterns cover areas up to 5 mm x 5 mm in size. The resolution is typically 400 nm over large areas and 200 nm over small areas. The resolution is currently limited due to the presence of primary particle clusters that are up to 400 nm in size. The sonication is insufficient to break up these clusters. We noticed that the cluster size increased over time in the non-polar solvent; high resolution was only obtained using fresh suspensions.

Figure 5 shows representative images of nanoxerographic printing onto these charge patterns. The images show patterns of gold (Fig. 5A), silver (Fig. 5B), and indium (Fig. 5C) nanoparticles that assembled on positively and negatively charged areas from the gas phase. The resolution achieved is 100 nm for the silver and indium particles and 200 nm for the gold nanoparticles.

The electrometer reading and the global electric field are two important parameters to control the assembly process, the coverage, the particle polarity that assembles on the surface, and the speed of the assembly. We observed a clear proportionality between the electrometer reading and the coverage. Excellent coverage and high selectivity were obtained when $\pm$4 nC of charged silver particles or $\pm$1 nC of charged indium particles accumulated on the sample, whereas at $\pm$10 nC the sample would be fully coated. The global electric field controls the polarity of assembled particles. Nanoparticles assembled well on positively charged areas (Figs. 5B,C) by applying a negative potential to the top electrode, whereas for negatively charged areas (Fig. 5A) a positive potential was required. The global electric field also effected how fast the assembly took place. At $\pm$1 kV and 1100 °C, the assembly time to get good coverage for silver at a flow rate of 1000 ccm was 1 minute whereas at $\pm$100V it took 10

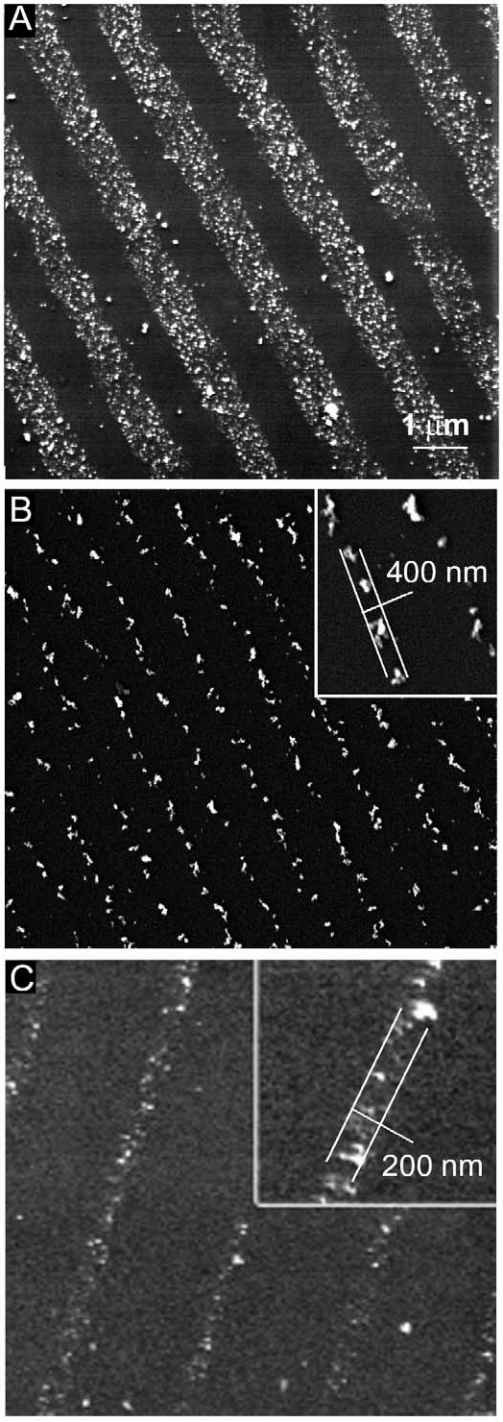

Figure 4: SEM images of graphitized carbon nanoparticles assembled from the liquid phase. (A) Assembly of particles on 1 μm wide positively charged lines. (B, C) Assembly of particles on areas patterned with 200 nm wide lines; the cluster size determines the width of the assembled lines.

minutes to get the same coverage. The assembly of the indium particles took place at a higher deposition rate than the silver particles. This could possibly be explained by the higher vapor pressure of indium at the evaporation temperature. The assembly time was 20 seconds at -1kV and 2 minutes at -100V.

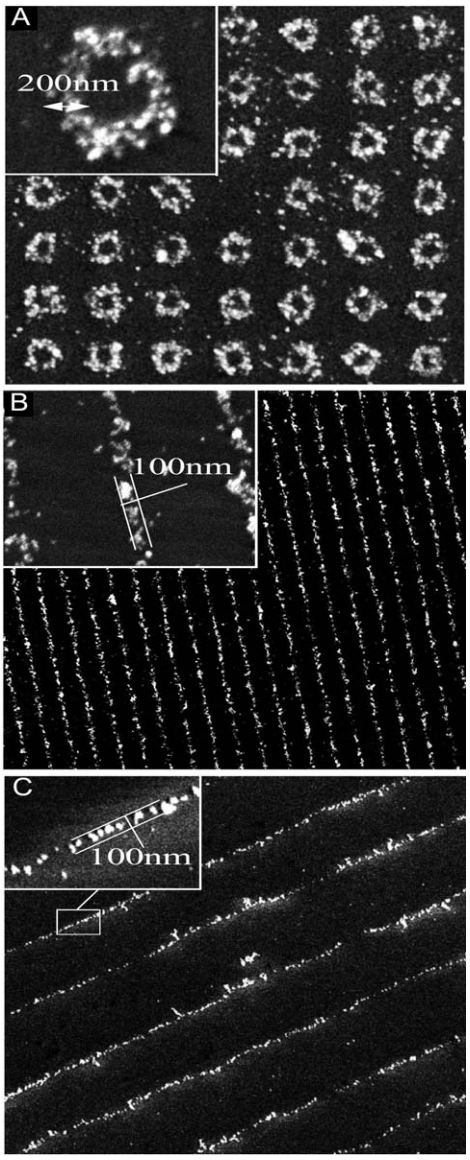

Figure 5: SEM images of different nanoparticle assemblies. Images (A,B) were patterned using PDMS electrodes, while image (C) was patterned with the thin silicon electrode. (A) Gold nanoparticles assembled onto negatively charged 200 nm wide rings. (B) Silver nanoparticles and (C) indium nanoparticles assembled onto positively charged 100 nm wide lines.

In conclusion, we have demonstrated nanoxerogaphic printing of different nanoparticles from the liquid and gas-phase with a resolution of 100 - 200 nm. Nanoxerography relies on a high resolution charge patterning technique, electric nanocontact printing, which is based on a flexible electrode structure that forms multiple electric contacts of different size and shape to an electret surface. The resolution of the developed technique is currently limited by the smallest possible feature size on the electrode structure. For the PDMS based electrode structure this limit is approx. 100 nm. Smaller features tend to collapse. Higher resolution might become possible using the proposed thin silicon, which is capable of supporting ~10 nm sized features[26]. The first results of nanoxerogaphic printing using the thin silicon are very encouraging. Whether nanoxerography will enable the printing of nanoparticle based devices remains to be shown. However, nanoxerogaphy offers a very competitive strategy compared to other techniques. It can handle all kinds of materials, is parallel, and could potentially accomplish 10 nm scale resolution or better.

Acknowledgements

The authors are pleased to acknowledge the financial support for the research by the National Science Foundation (DMI 0217538).

REFERENCES

[1] M. L. Ostraat, J. W. De Blauwe, M. L. Green, L. D. Bell, M. L. Brongersma, J. Casperson, R. C. Flagan, and H. A. Atwater, Applied Physics Letters **79,** 433-435 (2001).

[2] M. H. Nayfeh, S. Rao, N. Barry, J. Therrien, G. Belomoin, A. Smith, and S. Chaieb, Applied Physics Letters **80,** 121-123 (2002).

[3] G. Belomoin, J. Therrien, A. Smith, S. Rao, R. Twesten, S. Chaieb, M. H. Nayfeh, L. Wagner, and L. Mitas, Applied Physics Letters **80,** 841-843 (2002).

[4] C. Thelander, M. H. Magnusson, K. Deppert, L. Samuelson, P. R. Poulsen, J. Nygard, and J. Borggreen, Applied Physics Letters **79,** 2106-2108 (2001).

[5] T. Junno, M. H. Magnusson, S.-B. Carlsson, K. Deppert, J.-O. Malm, L. Montelius, and L. Samuelson, Microelectronic Engineering **47,** 179-183 (1999).
[6] T. W. Kim, D. C. Choo, J. H. Shim, and S. O. Kang, Applied Physics Letters **80,** 2168-2170 (2002).
[7] S. A. Maier, M. L. Brongersma, P. G. Kik, S. Meltzer, A. A. G. Requicha, and H. A. Atwater, Advanced Materials (Weinheim, Germany) **13,** 1501-1505 (2001).
[8] C. Baur, A. Bugacov, B. E. Koel, A. Madhukar, N. Montoya, T. R. Ramachandran, A. A. G. Requicha, R. Resch, and P. Will, Nanotechnology **9,** 360-364 (1998).
[9] W. A. Lopes and H. M. Jaeger, Nature **414,** 735-738 (2001).
[10] J. Janin, Progress in Biophysics & Molecular Biology **64,** 2-3 (1995).
[11] C. M. Niemeyer, B. Ceyhan, S. Gao, L. Chi, S. Peschel, and U. Simon, Colloid & Polymer Science **279,** 68-72 (2001).
[12] P. D. Yang, A. H. Rizvi, B. Messer, B. F. Chmelka, G. M. Whitesides, and G. D. Stucky, Advanced Materials **13,** 427-431 (2001).
[13] C. Petit, A. Taleb, and M. P. Pileni, Advanced Materials **10,** 259 ff. (1998).
[14] W. M. D. Wright and D. G. Chetwynd, Nanotechnology **9,** 133-142 (1998).
[15] H. O. Jacobs and A. Stemmer, Surface & Interface Analysis **27,** 361-367 (1999).
[16] H. O. Jacobs and G. M. Whitesides, Science **291,** 1763-1766 (2001).
[17] A. Born and R. Wiesendanger, Applied Physics a **68,** 131-135 (1999).
[18] H. O. Jacobs, S. A. Campbell, and M. G. Steward, Advanced Materials **14,** 1553-1557 (2002).
[19] C. R. Barry, M. G. Steward, N. Z. Lwin, and H. O. Jacobs, Nanotechnology **14,** 1057 (2003).
[20] R. Groff, P. Khargonekar, D. Koditschek, T. Thieret, and L. K. Mestha, Proceedings of the 38th IEEE Conference on Decision and Control **2** (1999).
[21] D. M. Pai and B. E. Springett, Reviews of Modern Physics **65,** 163-211 (1993).
[22] Y. Xia and G. M. Whitesides, Angewandte Chemie-International Edition England **37,** 550 (1998).
[23] T. W. Odom, J. C. Love, D. B. Wolfe, K. E. Paul, and G. M. Whitesides, Langmuir **18,** 5314-5320 (2002).
[24] H. O. Jacobs, H. F. Knapp, S. Muller, and A. Stemmer, Ultramicroscopy **69,** 39-49 (1997).
[25] H. O. Jacobs, P. Leuchtmann, O. J. Homan, and A. Stemmer, Journal of Applied Physics **84,** 1168-1173 (1998).
26 S. Y. Chou, C. Keimel, and J. Gu, Nature (London, United Kingdom) 417, 835-837 (2002).